^{11}C-flumazenil (FMZ) and noted that the distribution volume (receptor binding) of FMZ was not affected in the parietal cortex where metabolic defect was detected with FDG in Alzheimer's subjects. The reason for the difference between the FMZ binding data and our data is unclear. The difference in binding characteristics between the two ligands, IMZ and FMZ must be considered. For example, IMZ has a tenfold higher affinity for its binding than FMZ at 37°C and the nonspecific uptake of FMZ is much higher than that for IMZ (*24*).

We could not include an adequate number of normal subjects, since all the patients were studied as a part of a Phase II or III clinical trial of IMZ in Japan (*25,26*). Therefore, to assess the diagnostic value of this new radiopharmaceutical, a greater number of normal individuals should be studied.

CONCLUSION

IMZ-SPECT may be useful for the evaluation of the disease. The decline in Bz receptor density might provide a more accurate estimate of disease progression than reduction in rCBF.

ACKNOWLEDGMENTS

The authors thank Nihon Medi-Physic Co., Ltd. for providing the [^{123}I] Iomazenil.

REFERENCES

1. Holman BL, Johnson KA, Gerada B, Carvalho PA, Satlin A. The scintigraphic appearance of Alzheimer's disease: A prospective study using technetium-99m-HMPAO-SPECT. *J Nucl Med* 1992;33:181–185.
2. Cross AJ, Crow TJ, Ferrier IN, Johnson JA. The selectivity of the reduction of serotonin S2 receptors in Alzheimer-type dementia. *Neurobiol Aging* 1985;7:3–7.
3. Griffiths PD, Crossman AR. Receptor changes in the neocortex of postmortem tissue in Parkinson's disease and Alzheimer's disease. *Dementia* 1992;3:239–246.
4. Beer H, Bläuenstein PA, Hasler PH, et al. In vitro and in vivo evaluation of iodine-123-Ro 16–0154: A new imaging agent for SPECT investigations of benzodiazepine receptors. *J Nucl Med* 1990;31:1007–1014.
5. Cordes M, Henkes H, Ferstl F, et al. Evaluation of focal epilepsy: A SPECT scanning comparison of ^{123}-I-iomazenil versus HMPAO. *AJNR* 1992;13:249–253.
6. Huffelen AC, Veelen JW. Identification of the side of epileptic focus with ^{123}I-iomazenil SPECT. A comparison with ^{18}F-FDG-PET and ictal EEG findings in patients with medically intractable complex partial seizures. *Acta Neurochir* 1990; 50(suppl):95–99.
7. Shimohama S, Taniguchi T, Fujiwara M, Kameyama M. Changes in benzodiazepine receptors in Alzheimer-type dementia. *Ann Neurol* 1988;23:404–406.
8. Mckhann G, Drachman D, Folsteinal M, Katzman R, Price P, Stadlar EM. Clinical diagnosis of Alzheimer's disease: Report of the NINCDS-ADRDA work group under the auspices of the department of health and human services task force on Alzheimer's disease. *Neurology* 1984;34:939–944.
9. Kimura K, Hashikawa K, Etani H, et al. A new apparatus for brain imaging: four-head rotating gamma camera single-photon emission computed tomography. *J Nucl Med* 1990;31:603–609.
10. Schubiger PA, Hasler PH, Beer-Wohlfahrt H, et al. Evaluation of a multicenter study with iomazenil—a benzodiazepine receptor ligand. *Eur J Nucl Med* 1991;12:569–582.
11. Yonekura Y, Nishizawa S, Tanaka F, et al. Phase 1 clinical study of ^{123}I-iomazenil: a new probe to evaluate central-type benzodiazepine receptor with SPECT. *Jpn J Nucl Med* 1995;32:87–97.
12. Aquiloniws S, Eckerns A. *A color atlas of the human brain.* New York: Raven Press, 1980.
13. Onishi Y, Yonekura Y, Nishizawa, et al. Noninvasive quantification of iodine-123-iomazenil SPECT. *J Nucl Med* 1996;37:374–378.
14. Woods SW, Seibyl JP, Goddard AW, et al. Dynamic SPECT imaging after injection of the benzodiazepine receptor ligand [^{123}I] iomazenil in healthy human subjects. *Psych Res Neuroimag* 1992;45:67–77.
15. Lassen NA, Andersen AR, Friberg L, Paulson OB. The retention of [99mTc]-d,l-HM-PAO in the human brain after intracarotid bolus injection: a kinetic analysis. *J Cereb Blood Flow Metab* 1988;8:S13–S22.
16. Lear JL, Ackermann RF, Kameyama M, Kuhl DE. Evaluation of [^{123}I] isopropyliodo-amphetamine as a tracer for local cerebral blood flow using direct autoradiographic comparison. *J Cereb Blood Flow Metab* 1982;2:179–185.
17. Friedland RP, Brun A, Budinger TF. Pathological and positron emission tomographic correlation in Alzheimer's disease. *Lancet* 1985;1:228.
18. Hendry SHC, Schwark HD, Jones EG, Yan J. Numbers and proportions of GABA-immunoreactive neurons in different areas of monkey cerebral cortex. *J Neurosci* 1987;7:1503–1519.
19. Laruelle M, Baldwin RM, Rattner Z, et al. SPECT quantification of [123I] iomazenil binding to benzodiazepine receptors in nonhuman primates: I. kinetic modeling of single bolus experiments. *J Cereb Blood Flow Metab* 1994;14:439–452.
20. Abi-Dargham A, Laruelle M, Seibyl J, et al. SPECT measurement of benzodiazepine receptors in human brain with iodine-123-iomazenil: kinetic and equilibrium paradigms. *J Nucl Med* 1994;35:228–238.
21. Onishi Y, Yonekura Y, Mukai T, et al. Simple quantification of benzodiazepine receptor binding and ligand transport using iodine-123-iomazenil and two SPECT scans. *J Nucl Med* 1995;36:1201–1210.
22. Weinberger DR, Gibson R, Coppola R, et al. The distribution of cerebral muscarinic acetylcholine receptors in vivo in patients with dementia: a controlled study with ^{123}IQNB and single-photon emission computed tomography. *Arch Neurol* 1991;48: 169–176.
23. Meyer MA, Koeppe RA, Frey KA, Foster NL, Kuhl DE. Positron emission tomography measures of benzodiazepine binding in Alzheimer's disease. *Arch Neurol* 1995;52:314–317.
24. Johnson EW, Woods SW, Zoghbi S, McBride BJ, Baldwin RM, Innis RB. Receptor binding characterization of the benzodiazepine radioligand ^{125}I-Ro16–0154: potential probe for SPECT brain imaging. *Life Sci* 1990;47:1535–1546.
25. Torizuka K, Uemura K, Tohru M, et al. Phase 2 clinical study of ^{123}I-iomazenil in various cerebral disease: part 2. Clinical evaluation of central-type benzodiazepine receptor imaging with ^{123}I-iomazenil SPECT. *Jpn J Nucl Med* 1996;33:191–205.
26. Torizuka K, Uemura K, Tohru M, et al. Phase 3 clinical study of ^{123}I-Iomazenil, a new central-type benzodiazepine receptor imaging agent (part 2): report on clinical usefulness in diagnosis of degenerative neurological diseases and mental disorders. *Jpn J Nucl Med* 1996;33:303–318.

Brain Dopamine Transporter in Spontaneously Hypertensive Rats

Yoshiyuki Watanabe, Masahiro Fujita, Yasushi Ito, Tomoya Okada, Hideo Kusuoka and Tsunehiko Nishimura

Division of Tracer Kinetics, Biomedical Research Center Osaka University Medical School, Osaka, Japan

The brain dopamine system plays an important role in the development of hypertension. **Methods:** The amounts of the dopamine transporter (DAT) and dopamine D1 and D2 receptors in the brain were assessed by in vitro autoradiography with the ligands [^{125}I]β-CIT, [^{125}I]SCH23982 and [^{125}I]iodospiperone, respectively. Changes in this transporter and the two receptors were evaluated in spontaneously hypertensive (SH) rats and control (Wistar-Kyoto) rats at the prehypertensive (2-wk-old, n = 5) and posthypertensive (15-wk-old, n = 5) stages. **Results:** The β-CIT binding for the DAT was increased significantly in the caudate-putamen (CPu) of SH rats compared with that of Wistar-Kyoto (WKY) rats at both pre- and posthypertensive stages. In the evaluation of the lateral-to-medial CPu, the β-CIT binding on the lateral side was significantly higher than that on the medial side in SH rats at 2 wk. The SCH23982 binding for D1 receptor was increased significantly in CPu at posthypertensive SH rats. **Conclusion:** Increased DAT was found before the development of hypertension, and the increased DAT and D1 receptor were found at posthypertensive SH rats. The abnormal dopamine system contributes the development of hypertension, suggesting the possibility of diagnostic imaging for the essential hypertension.

Key Words: hypertension; iodine-125-β-CIT; dopamine transporter; dopamine receptor

J Nucl Med 1997; 38:470–474

Received Jan. 16, 1996; revision accepted Jun. 13, 1996.

For correspondence or reprints contact: Yoshiyuki Watanabe, MD, Division of Tracer Kinetics, Biomedical Research Center, Osaka University Medical School, 2-2 Yamadaoka Suita, Osaka 565, Japan.

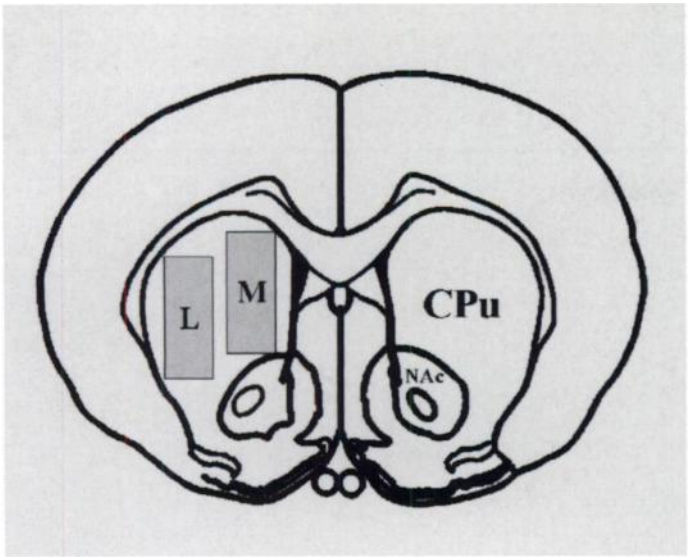

FIGURE 1. ROI in a striatal section where specific binding of the lateral or medial CPu was measured. This selected section was located at about 1.0 mm rostral from the bregma. CPu = caudate-putamen; NAc = nucleus accumbens; L = ROI of the lateral CPu; M = ROI of the medial CPu.

The brain dopamine systems, especially the nigrostriatal pathway, play a direct role in the regulation of blood pressure and the development of hypertension. Chemical or electrolytic lesions of the nigrostriatal dopamine system in spontaneously hypertensive (SH) rats during the prehypertensive stage attenuate the development of hypertension (*1,2*). Moreover, elevated tyrosine hydroxylase activity (*3*) and higher dihydroxyphenylacetic acid (DOPAC) concentrations (*4,5*) have been reported in the striatum of SH rats. These results suggest that the nigrostriatal dopamine system in SH rats is hyperactive and that this hyperactivity causes the development of hypertension.

SH rats are generally considered to be a suitable experimental model for the study of human essential hypertension (*6*) and to have some similarities in the dysfunction of the central dopamine system. The dopamine D2 receptor agonist, bromocriptine, decreases blood pressure in SH rats and in patients with essential hypertension, and both SH rats and some patients with essential hypertension show high plasma prolactin levels (*7,8*).

To elucidate the hypertension-related alteration of dopamine systems in brain, we compared the amounts of DAT, D1 and D2 receptors between SH rats and control (Wistar-Kyoto) rats at the prehypertensive stage (2-wk-old) and after the development of hypertension (15-wk-old).

MATERIALS AND METHODS

Male SH rats and Wistar-Kyoto (WKY) rats at age 2 or 15 wk were examined. The rats were housed under a constant light-dark cycle with standard pellet food and tap water available ad libitum. Blood pressure was measured on conscious animals with a tail-cuff method.

After anesthetization using sodium pentobarbital (50 mg/kg weight intraperitoneally), the brain was removed rapidly and frozen on a cryostat chuck using crushed dry ice. In a cryostat microtome, 20-μm sections were cut and mounted onto silane-coated slides. The glass slides were stored at −80°C until use.

Autoradiographic Investigations

[^{125}I]2β-carbomethoxy-3β-(4-iodophenyl)tropane (β-CIT, also referred to as RTI-55: 2200 Ci/mmole; Dupont-NEN, Boston, MA) was used to label DAT in the rat brain as described previously (*9*) with slight modification. The slides were preincubated in 50 m*M* Tris-HCl buffer (pH 7.4) containing 100 m*M* NaCl at 4°C for 10 sec and incubated in the buffer containing 100 p*M* [^{125}I]β-CIT and 100 n*M* clomipramine (Research Biomedical, Natick, MA) for 2 hr at 4°C to measure total binding. Nonspecific binding was evaluated by including 300 m*M* (−)-cocaine in incubation media. Clomipramine was added to displace serotonin transporters. Incubation was terminated by two consecutive 1-min washes in fresh ice-cold buffer and dipped in ice-cold distilled water. In this study, the concentration of (−)-cocaine and clomipramine was diluted to one-third and one-hundredth, respectively. The preliminary study showed the good displacement of dopamine and serotonin transporters by diluted (−)-cocaine or clomipramine buffers.

Autoradiography with [^{125}I]SCH23982 (R(+)-8[^{125}I]-iodo-7-hydroxy-2,3,4,5-tetrahydro-3-methyl-5-phenyl-1H-3-benzazepine 2200 Ci/mmole; Dupon-NEN, Boston, MA) was carried out as described previously (*10*). In brief, the slides were incubated at 22°C for 30 min in 50 m*M* Tris-HCl buffer (pH 7.4) containing 120 m*M* NaCl, 5 m*M* KCl, 2 m*M* $CaCl_2$, 1 m*M* $MgCl_2$, 50 n*M* ketanserin (Research Biochemical, Natick, MA) and 100 p*M* [^{125}I]SCH23982. Nonspecific binding was evaluated by including 100 n*M* unlabeled SCH23982 (Research Biochemical, Natick, MA) in incubation media. Ketanserin was used to displace the binding to serotonin receptors. After an incubation period, the slides were rinsed in ice-cold buffer twice for 5 min each and washed with distilled water for a few seconds.

Autoradiography with [^{125}I]iodospiperone (2200 Ci/mmole; Dupon-NEN, Boston, MA) was performed as follows. The slides were incubated at 22°C for 60 min in 50 m*M* Tris-HCl (pH 7.4) containing 100 m*M* NaCl, 100 n*M* ketanserin and 250 p*M* [^{125}I]iodospiperone. Nonspecific binding was assessed by including 250

TABLE 1
General Characteristics of Experimental Rats

	2-wk-old		15-wk-old	
	WKY	SHR	WKY	SHR
Body weight (g)	32.0 ± 1.0	26.0 ± 0.9*	315 ± 1.0	302 ± 2.1*
Blood pressure (mmHg)	—	—	125 ± 5.2	172 ± 2.1*

*$p < 0.005$ vs WKY.
Each value is the mean ± s.e.m. in five rats.
The blood pressure of 2-wk-old rats was not available because they were too small to measure by tail-cuff method.

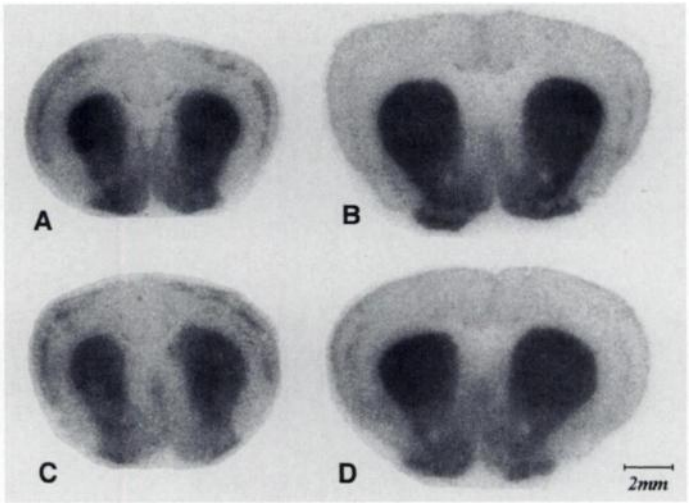

FIGURE 2. Autoradiograms of [^{125}I]β-CIT in the striatum. A = 2-wk-old SH rats; B = 15-wk-old SH rats; C = 2-wk-old WKY rats; D = 15-wk-old WKY rats.

TABLE 2
Iodine-125-β-CIT Binding Density in the Brain

	2-wk-old		15-wk-old	
	WKY	SHR	WKY	SHR
Iodine-125-β-CIT (fmole/mg tissue)				
Caudate-Putamen	2.12 ± 0.07	2.33 ± 0.07*	3.75 ± 0.11	4.37 ± 0.11†
Lateral	2.53 ± 0.12	2.84 ± 0.12‡	4.26 ± 0.17†	4.88 ± 0.18*‡
Medial	2.48 ± 0.11	2.67 ± 0.11	3.93 ± 0.16	4.41 ± 0.16*
Nucl. Accumbens	1.81 ± 0.09	1.92 ± 0.06	2.77 ± 0.14	3.15 ± 0.15

*$p < 0.05$
†$p < 0.005$ vs. WKY
‡$p < 0.005$ vs. medial side
Each value is the mean ± s.e.m. in five rats.

n*M* spiperone hydrochloride (Research Biochemical, Natick, MA) in incubation media. Ketanserin was added to prevent [^{125}I]iodospiperone from binding to serotonin receptors. The slides were washed twice with ice-cold buffer for 5 min each and washed once with distilled water for a few seconds.

Image Analysis

The labeled tissues along with [^{125}I]microscales standard (Amersham, Buckinghamshire, England) were placed against sheets of imaging film (X-OMAT AR, Kodak, Tokyo, Japan) in radiograph cassettes. After 12 to 48 hr exposure, films were removed and developed. The films were quantified using a computer-based analysis system (MCID Image Analysis System, Imaging Research, St. Catharines, Ontario, Canada). The film optical densities were converted to fmole/mg tissue using a standard curve generated by the [^{125}I]microscale. Two in vitro autoradiography experiments were performed with each radioligand and their average value was calculated.

The binding density was obtained over the whole area of the caudate-putamen (CPu) and the nucleus accumbens (NAc). The binding densities in five sections in each 2-wk-old rat and six sections in each 15-wk-old rat were measured. Two sections in the central area (in the rostral-caudal directions) of CPu were selected to compare the amounts of each radioligand in the lateral and the medial CPu. Two rectangular ROIs were selected in the lateral and the medial CPu (Fig. 1). The two selected sections were contiguous with Plates 14 or 17 in the atlas by Paxinos and Watson (*11*).

Statistical Analysis

Data are presented as mean ± s.e.m. The binding densities in SH rats were compared to those in WKY rats using the Mann-Whitney U test. The values in the lateral CPu were compared to those in the medial CPu using Wilcoxon signed-ranks test. The probability level of less than 0.05 was considered statistically significant.

RESULTS

The age-related changes in body weight and blood pressure are shown in Table 1.

Specific Binding of Iodine-125-β-CIT

Figure 2 shows the binding of [^{125}I]β-CIT in the brains of SH rats and WKY rats. Compared to WKY rats (C, D), SH rats (A, B) showed higher [^{125}I]β-CIT binding in CPu at both 2 and 15 wk. The [^{125}I]β-CIT binding sites in CPu were homogeneous and did not show different distributions in the striosome and matrix compartments. Table 2 summarizes the quantitative specific binding of [^{125}I]β-CIT in CPu and NAc. The binding density in SH rats was significantly increased in CPu at 2 wk ($p < 0.05$) and 15 wk ($p < 0.005$) compared to WKY rats.

Compared to the medial CPu, the [^{125}I]β-CIT binding in the lateral CPu was significantly greater in 15-wk-old rats of both strains ($p < 0.005$). In the 2-wk-old rats, this lateral-to-medial gradient was found only in SH rats ($p < 0.005$) but not in WKY rats. In both the lateral and the medial CPu, the [^{125}I]β-CIT

TABLE 3
Iodine-125-SCH23982 and Iodine-125-Iodospiperone Binding Density in the Brain

	2-wk-old		15-wk-old	
	WKY	SHR	WKY	SHR
Iodine-125-SCH23982 (fmole/mg tissue)				
Caudate-Putamen	3.70 ± 0.07	3.67 ± 0.07	3.36 ± 0.08	3.78 ± 0.10†
Lateral	3.91 ± 0.10	3.92 ± 0.11	3.19 ± 0.11	3.60 ± 0.12*‡
Medial	3.78 ± 0.09	3.70 ± 0.09	3.12 ± 0.09	3.45 ± 0.10*
Nucl. accumbens	3.57 ± 0.07	3.47 ± 0.11	2.77 ± 0.14	3.15 ± 0.15
Iodine-125-iodospiperone (fmole/mg tissue)				
Caudate-Putamen	6.63 ± 0.27	6.23 ± 0.29	6.69 ± 0.32	7.35 ± 0.36
Lateral	8.31 ± 0.36‡	7.93 ± 0.47‡	8.37 ± 0.53‡	7.92 ± 0.52‡
Medial	6.53 ± 0.31	6.55 ± 0.42	7.12 ± 0.43	6.64 ± 0.47
Nucl. accumbens	4.59 ± 0.33	4.63 ± 0.49	6.19 ± 0.46	6.00 ± 0.54

*$p < 0.05$
†$p < 0.005$ vs. WKY
‡$p < 0.005$ vs. medial side
Each value is the mean ± s.e.m. in five rats.

binding in SH rats was significantly greater than that in WKY rats at 15 wk ($p < 0.05$).

Specific Binding of Iodine-125 SCH23982 and Iodine-125 Iodospiperone

Table 3 summarizes the quantitative specific binding of [^{125}I]SCH23982 and [^{125}I]iodospiperone in CPu and NAc. The [^{125}I]SCH23982 binding in CPu was significantly increased in SH rats only at age 15 wk ($p < 0.005$) compared to WKY rats. There was no significant difference between SH rats and WKY rats at either age in [^{125}I]iodospiperone binding. In NAc, the binding densities showed no difference in the two strains for either tracer.

In both the lateral and the medial CPu, the [^{125}I]SCH23982 binding in 15-wk-old SH rats was significantly greater compared to WKY rats ($p < 0.05$). In addition, the lateral-to-medial gradient of [^{125}I]SCH23982 binding was detected only in 15-wk-old SH rats ($p < 0.005$). The [^{125}I]iodospiperone binding in the lateral CPu was significantly greater than that in the medial CPu at both ages and in both strains ($p < 0.005$).

DISCUSSION

This study demonstrates the increased DAT in the CPu of both pre- and posthypertensive SH rats. In the prehypertensive SH rats, the difference between SH rats and WKY rats was found only by the ligand of DAT. That is, the increase of total amount in CPu and the expression of lateral-to-medial gradient. These results suggest that these changes may be inherent and pathogenetic to hypertension and indicate that it may be possible to detect an abnormality in DAT with in vivo imaging even before the development of hypertension.

SH rats were bred from the WKY rats by selective brother-to-sister inbreeding and uniformly result in offspring that develop hypertension (*12*). SH rats are similar to humans with respect to essential hypertension in several ways. Both have apparent onsets very early in life. Their elevated arterial pressure is mediated through a slow and progressively increased total peripheral resistance that demands cardiac and vascular adaptation (*13*).

In contrast to our findings, it was reported that there was no significant difference in DAT labeled with [^{3}H]mazindol between adult age-matched SH rats and Sprague-Dawley rats (*14*). The discrepancy between two studies may be due to the differences in radioligands and in the strain selected as the normotensive rat. Iodine-125-β-CIT may be different from [^{3}H]mazindol in the binding site and the affinity to DAT. The [^{3}H]mazindol binding in the striatum is differentially distributed in the striosome and matrix compartments (*15*). This inhomogeneity in the striatum is not observed in [^{125}I]β-CIT (*9,16,17*). Furthermore, [^{125}I]β-CIT binds to DAT at both high- and low-affinity sites in the striatum, similar to cocaine (*16*), but [^{3}H]mazindol binds to DAT only at one high-affinity binding site (*18*).

The lateral-to-medial gradient of DAT in CPu was found only in SH rats at age 2 wk but in both strains at 15 wk (Table 2). The lateral or medial portions of CPu differ in neurogenesis and in the development of dopaminergic innervation (*19,20*). In the striatum, the ingrowth of the mesencephalo-prosencephalic dopaminergic fibers is predominantly located laterally. From lateral portion, the outgrowth of the dopaminergic fibers proceeds in the medial direction (*19*). Thus, early expression of the lateral-to-medial gradient in DAT indicates an abnormal ontogenic development of the dopamine system in SH rats.

There are many previous reports describing dopamine D1 or D2 receptor binding studies in SH rats, but these results are confusing. Some researchers reported an increase of D1 or D2 receptor densities in the striatum of SH rats (*14,21–23*), whereas others reported that there was no difference between SH and WKY rats (*24–26*). The discrepancies in D1 and D2 receptor data have been attributed to the difference of radioligands and experimental procedures and to genetic drift resulting in biological variability among the substrains of SH rats (*27*).

Iodine-125-β-CIT has been used as a tracer for SPECT studies in baboons and humans (*28–33*). In recent years, the in vivo tracer kinetics (*34*) or age-related decline (*35*) in human striatum of [^{125}I]β-CIT have been investigated. Iodine-125-β-CIT is a promising SPECT agent for imaging the DAT in humans. Our study suggests the possibility of diagnostic imaging for essential hypertension.

CONCLUSION

The increased DAT was found before the development of hypertension in SH rats, and increased DAT and D1 receptor were found in posthypertensive SH rats. These results suggest that the dopamine system in the striatum plays an important role in the pathogenesis and development of hypertension.

REFERENCES

1. Buuse MV, Versteeg DHG, Jong WD. Brain dopamine depletion by lesion in the substantia nigra attenuates the development of hypertension in the spontaneously hypertensive rat. *Brain Res* 1986;368:69–78.
2. Linthorst ACE, Giersbergen PLM, Gras M, Versteeg DHG, Jong WD. The nigrostriatal dopamine system: role in the development of hypertension in spontaneously hypertensive rat. *Brain Res* 1994;639:261–268.
3. Nagaoka A, Lovenberg W. Regional changes in the activities of aminergic biosynthetic enzymes in the brains of hypertensive rats. *Eur J Pharmacol* 1977;43:297–306.
4. Howes LG, Rowe PR, Summers RL, Louis WJ. Age-related changes of catecholamines and their metabolites in central nervous system regions of spontaneously hypertensive and normotensive Wistar-Kyoto rats. *Clin Exp Hypert* 1984;A6:2263–2277.
5. McKeon TW, Hendly ED. Brain monoamines and metabolites in hypertensive and hyperactive rat strains. *Clin Exp Hypert* 1988;A10:971–994.
6. Yamori Y. Development of the spontaneously hypertensive rat and of various spontaneous rat models and their implications. In: Jong WD, ed. *Handbook of hypertension: experimental and genetic model of hypertension,* vol.4. Amsterdam, The Netherlands: Elsevier Science; 1984:224–239.
7. Stumpe KO, Kolloch R, Higuchi M, Kruck F, Vetter H. Hyperproloctinemia, antihypertensive effect of bromocriptine in essential hypertension. *Lancet* 1977:211–214.
8. Sowers JR. Effect of bromocriptine on responses to stress in spontaneously hypertensive rats. *Hypertension* 1981;3:544–550.
9. Fujita M, Shimada S, Fukuchi K, Tohyama M, Nishimura T. Distribution of cocaine recognition sites in rat brain: in vitro and ex vivo autoradiography with [^{125}I]RTI-55. *J Chem Neuroanat* 1994;7:13–23.
10. Dawson TM, Barone P, Sidhu A, Wamsley JK, Chase TN. The D1 dopamine receptors in the rat brain: quantitative autoradiographic localization using an iodinated ligand. *Neuroscience* 1988;26:83–100.
11. Paxinos G, Watson C. *The rat brain in stereotaxic coordinates.* San Diego, CA: Academic Press; 1986.
12. Okamoto K, Aoki K. Development of a strain of spontaneous hypertensive rats. *Jpn Circ J* 1963;27:282–293.
13. Trippodo NC, Frohlich ED. Similarities of genetic hypertension; man and rat. *Circ Res* 1981;48:309–319.
14. Kujirai K, Przendborski S, Kostic V, et al. Autoradiography of dopamine receptors and dopamine uptake sites in the spontaneously hypertensive rat. *Brain Res Bull* 1990;25:703–709.
15. Graybiel AM, Moratalla R. Dopamine uptake sites in the striatum are distributed differentially in striosome and matrix compartment. *Proc Natl Acad Sci USA* 1989;86:9020–9024.
16. Boja JW, Mitchell WM, Patel A, et al. High-affinity binding of [^{125}I]RTI-55 to dopamine and serotonin transporters in rat brain. *Synapse* 1992;12:27–36.
17. Cline EJ, Scheffel U, Boja JW, et al. In vivo binding of [^{125}I]RTI-55 to dopamine transporters: pharmacology and regional distribution with autoradiography. *Synapse* 1992;12:37–46.
18. Javitch JA, Blaustein RO, Snyder SH. [^{3}H]mazindol binding associated with neuronal dopamine and norepinephrine uptake sites. *Mol Pharmacol* 1984;26:35–44.
19. Voorn P, Kalsbeek A, Jorritsma-Byham B, Groenewegen HJ. The pre-, postnatal development of the dopaminergic cell groups in the ventral mesencephalon of the striatum of the rat. *Neuroscience* 1988;25:857–887.
20. Bayer SA. Neurogenesis in the rat striatum. *Int J Devl Neuroscience* 1984;2:163–175.
21. Kirouac GJ, Ganguly PK. Up-regulation of dopamine receptors in the brain of the spontaneous hypertensive rat: an autoradiography analysis. *Neuroscience* 1993;52:135–141.
22. Lim DK, Ito Y, Hoskins B, Rockhold RW, Ho IK. Comparative studies of muscarinic and dopamine receptors in three strains of rat. *Eur J Pharmacol* 1989;165:279–287.
23. Lim DK, Yu ZJ, Hoskins B, Rockhoid RW, Ho IK. Effect of acute and subacute cocaine administration on the CNS dopaminergic system in Wistar-Kyoto and

spontaneously hypertensive rats: 2 dopamine receptors. *Neurochem Res* 1990;15:621–627.
24. Watanabe M, Tsuruta S, Inoue Y, et al. Dopamine D1 and D2 receptors in spontaneously hypertensive rat brain striatum. *Can J Physiol Phamacol* 1989;67: 1596–1597.
25. Linthorst ACE, Jong WD, Boer TD, Versteeg DHG. Dopamine D1 and D2 receptors in the caudate nucleus of spontaneously hypertensive rats and normotensive Wistar-Kyoto rats. *Brain Res* 1993;602:119–125.
26. Buuse MV, Jones R, Wagner J. Brain dopamine D2 receptor mechanisms in spontaneously hypertensive rats. *Brain Res Bull* 1992;28:289–297.
27. Versteeg DHG, Petty MA, Bohus B. The central nervous system and hypertension: the role of catechoamines and neuropeptides. In: Jong WD, ed. *Handbook of hypertension: experimental and genetic model of hypertension*, vol. 4. Amsterdam, The Netherlands: Elsevier Science;1984:398–430.
28. Kaufman MJ, Madras BK. Distribution of cocaine recognition sites in monkey brain: 2. Ex vivo autoradiography with [^{3}H]CFT and [^{125}I]RTI-55. *Synapse* 1992;12:99–111.
29. Staley JK, Basile M, Flynn DD, Mash DC. Visualizing dopamine and serotonin transporters in the human brain with the potent cocaine analog [^{125}I]RTI-55: in vitro binding and autoradiographic characterization. *J Neurochem* 1994;62:549–556.
30. Seibyl JP, Wallace E, Smith EO, et al. Whole-body biodistribution, radiation absorbed dose and brain SPECT imaging with iodine-123-β-CIT in healthy human subjects. *J Nucl Med* 1994;35:764–770.
31. Kuikka JT, Bergstrom KA, Ahonen A, Lansimies E. The dosimetry of iodine-123-labeled 2β-carbomethoxy-3β-(4-iodophenyl)tropane. *Eur J Nucl Med* 1994;21:53–56.
32. Innis RB. Single-photon emission tomography imaging of dopamine terminal innervation: a potential clinical tool in Parkinson's disease. *Eur J Nucl Med* 1994;21:1–5.
33. Seibyl JP, Laruelle M, Dyck CH, et al. Reproducibility of iodine-123-β-CIT SPECT brain measurement of dopamine transporters. *J Nucl Med* 1996;37:222–228.
34. Laruelle M, Wallace E, Seibyl JP, et al. Graphical, kinetic and equilibrium analyses of in vivo [^{123}I]beta-CIT binding to dopamine transporters in healthy human subjects. *J Cereb Blood Flow Metab* 1994;14:982–994.
35. Dyck CH, Seibyl JP, Malison RT, et al. Age-related decline in striatal dopamine transporter binding with iodine-123-β-CIT SPECT. *J Nucl Med* 1995;36: 1175–1181.

(continued from page 7A)

FIRST IMPRESSIONS

Technetium-99m-Macroaggregated Albumin in Superior Vena Caval Obstruction

Figure 1.

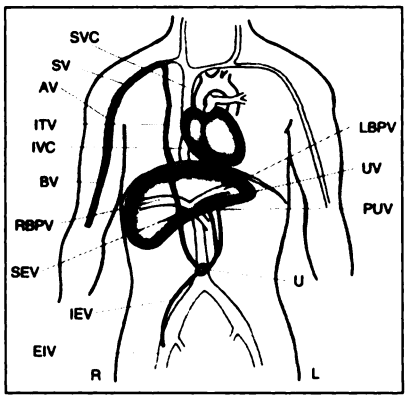

Figure 2.

PURPOSE

A 19-yr-old girl with acute lymphocytic leukemia and a known clot around her porta-cath central line was studied for suspected pulmonary embolism because of chest pain. After right arm intravenous injection of ^{99m}Tc-MAA, the perfusion lung scan (Fig. 1, anterior view) showed abnormal tracer activity below the diaphragm, in the left lobe of the liver, suggestive of superior vena caval (SVC) obstruction with collateral drainage into the systemic-portal venous blood flow to the left lobe of the liver. Right arm venogram done the same day confirmed SVC obstruction with collaterals and flow via the internal thoracic vein.

The demonstration of the left lobe of the liver suggests that the main route for collateral drainage, in this patient, is through the internal thoracic vein, the superior epigastric veins, the periumbilical venous channels and the umbilical and/or paraumbilical veins that drain into the left branch of the portal vein (Fig. 2, where AV = axillary vein, BV = brachial vein, EIV = external iliac vein, IEV = inferior epigastric vein, ITV = internal thoracic vein, IVC = inferior vena cava, L = left, LBPV = left branch of portal vein, PUV = paraumbilical vein, R = right, RBPV = right branch of portal vein, SEV = superior epigastric vein, SV = subclavian vein, SVC = superior vena cava and site of obstruction, U = umbilicus and periumbilical venous channels, UV = umbilical vein) and give rise to the tracer activity seen in the left lobe of the liver. In addition, the appearance of the liver also suggests that the major deep collateral flow through the azygos ascending lumbar pathway is less well developed.

TRACER

Technetium-99m-macroaggregated albumin, 3 mCi (111 MBq)

ROUTE OF ADMINISTRATION

Intravenous, right arm

TIME AFTER INJECTION

Ten minutes

INSTRUMENTATION

General Electric Starcam 3000 LFOV gamma camera with LEHR collimator

CONTRIBUTORS

Haim Golan, Judith M. Ash, Peter G. Chait and David L. Gilday, Division of Nuclear Medicine, Department of Diagnostic Imaging, The Hospital for Sick Children, Medicine, Toronto, Ontario, Canada